Kinetics study of C2+ oxygenates synthesis from syngas over Rh–MnOx/SiO2 catalysts

ARTICLE *in* CHEMICAL ENGINEERING SCIENCE · MARCH 2015

Impact Factor: 2.34 · DOI: 10.1016/j.ces.2015.02.035

9 AUTHORS, INCLUDING:

DongLong Fu

Utrecht University

4 PUBLICATIONS **4** CITATIONS

SEE PROFILE

Yi-Fan Han

East China University of Science and Techn…

63 PUBLICATIONS **1,812** CITATIONS

SEE PROFILE

Chemical Engineering Science 135 (2015) 301–311

Contents lists available at ScienceDirect

Chemical Engineering Science

journal homepage: www.elsevier.com/locate/ces

A mechanistic basis for the effects of Mn loading on C_{2+} oxygenates synthesis directly from syngas over Rh–MnO_x/SiO_2 catalysts

Wei Mao, Junjie Su, Zhengpai Zhang, Xin-Chao Xu, Donglong Fu, Weiwei Dai, Jing Xu *, Xinggui Zhou, Yi-Fan Han *

State Key Laboratory of Chemical Engineering, East China University of Science and Technology, Shanghai 200237, China

HIGHLIGHTS

- The intrinsic kinetics of CO hydrogenation over Rh–MnO_x catalysts was established.
- The E_a for CH_4 increased rapidly, but changed little for ethanol when adding MnO_x.
- CO dissociation is enhanced by tilted CO adsorption on Rh–MnO_x interface.
- Linearly adsorbed CO on $Rh^{\delta+}$ sites promoted CO insertion over Rh–MnO_x catalysts.

GRAPHICAL ABSTRACT

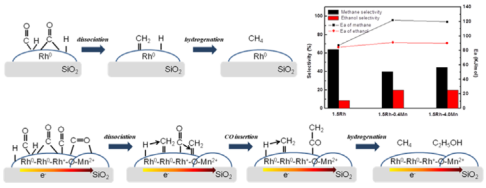

ARTICLE INFO

Article history:
Received 13 December 2014
Received in revised form
3 March 2015
Accepted 14 March 2015
Available online 27 March 2015

Keywords:
Rhodium
C_{2+} oxygenates
Intrinsic kinetics
Syngas
MnO_x promotional effect
Mechanism

ABSTRACT

Kinetics of the synthesis of C_{2+} oxygenates directly from syngas was investigated over a series of Rh–MnO_x/SiO_2 catalysts (atomic ratio of Mn/Rh=0, 0.5 and 5.0). It was evidenced that the activation energies for C_{2+} oxygenates changed little when introducing MnO_x, while the apparent activation energies for hydrocarbons, especially methane, increased remarkably. Kinetic parameters indicate that the formation of hydrocarbons can be suppressed in the presence of MnO_x. In the meantime, the reaction orders with respect to different products were also altered with the variation of MnO_x loadings. In accordance with in situ DRIFTS, we found that two new active sites on Rh surfaces resulting from the Rh–MnO_x interaction might be responsible for the enhancement of reaction rates and the selectivity to C_{2+} oxygenates. However, the over-loading of MnO_x leads to a decrease in the number of active sites.

1. Introduction

The synthesis of liquid fuels based on non-oil fossil resources (coal, biomass and natural (shale and tight) gas) from CO hydrogenation has been attracting to industry since 1920s. But it was not until 1970s since Bhasin et al. (1978) reported that C_{2+} oxygenates (ethanol, acetaldehyde and acetic acid) could be produced through this process over particular supported metal catalysts under well-controlled conditions. Among those products, acetaldehyde and acetic acid can be transferred into ethanol through a sequential catalytic hydrogenation. Since ethanol can be used as a fuel additive or a fuel alternative due to its high octane number, such a process has been regarded as an effective pathway for the clean utilization of non-oil fossil fuels.

Recent reviews show that several types of catalysts have been investigated for this process, including rhodium (Rh)-based catalysts, molybdenum sulfide-based catalysts, modified Fischer–Tropsch (F–T) catalysts and modified methanol synthesis catalysts (Farrell et al., 2006; Spivey and Egbebi, 2007; Subramani and Gangwal, 2008; Zaman and Smith, 2012). Among those catalysts,

* Corresponding authors. Tel./fax: +86 21 64251928.
E-mail addresses: xujing@ecust.edu.cn (J. Xu), yifanhan@ecust.edu.cn (Y.-F. Han).

http://dx.doi.org/10.1016/j.ces.2015.03.023
0009-2509/

supported Rh catalysts (usually ca. 5.0 wt% Rh) exhibited higher selectivity, especially to alcohols; however, they are still unfeasible for practical applications because of the high cost of Rh and relatively low catalytic efficiency.

In order to reduce the consumption of Rh and maximize the catalytic efficiency over the catalyst, various electronic promoters, such as Li (Schwartz et al., 2011), V (Gao et al., 2009a, 2009b), La (Subramanian et al., 2010), Fe (Chen et al., 2011), and Mn (Yin et al., 2003) were investigated. Previous studies have demonstrated that the performance of Rh catalysts could be enhanced significantly with the modification of MnO_x. Lisitsyn et al. (1990) and Sachtler and Ichikawa (1986) proposed that MnO_x might boost CO dissociation through the formation of tilted CO adsorbed at the interface of Rh–MnO_x. van den Berg et al. (1985) and Ojeda et al. (2004) suggested that the MnO_x might act as an electron-withdrawing promoter, which partially oxidizes the Rh atoms at the interface of Rh–MnO_x to enhance the CO insertion in the aim reaction.

The Goodman group (McClure et al., 2011) has demonstrated that the optimum size of Rh particles was ~2.5 nm for CO hydrogenation over a model Rh/SiO_2 catalyst. By DFT calculations, Choi and Liu (2009) demonstrated that CO hydrogenation was impeded due to the strong Rh–CO bond on Rh(1 1 1), which depressed the formation of ethanol. More recently, Ma et al. (2011) proved that MnO_x could stabilize both intermediates and reaction products. However, due to the so-called "material gap" from model to technical catalysts, those assertions are hard to be a guidance for the design of industrial or technical catalysts. Furthermore, despite the intensive kinetic studies of F–T synthesis, the intrinsic kinetics of C_{2+} oxygenates synthesis from syngas over Rh based catalysts under real reaction conditions (250–300 °C, 2.0–5.0 MPa) have still been rarely reported.

In the present study, as a part of the efforts to the mechanistic investigation of the aiming reaction system, the intrinsic kinetics for C_{2+} oxygenates synthesis directly from syngas was studied using a series of Rh–MnO_x/SiO_2 catalysts with a fixed Rh loading and different MnO_x loadings. We aim to reveal the effects of different MnO_x loadings on the performance of Rh catalysts. The kinetic measurements of CO hydrogenation in the temperature range 230–290 °C were carried out under real reaction conditions. Finally, with the combination of catalyst structures and kinetic parameters, the structure–performance relationship, in particular, the Rh catalytic property promoted by MnO_x, was discussed.

2. Experimental section

2.1. Catalyst preparation

For the catalyst preparation, aqueous solutions of $Rh(NO_3)_3$ (Heraeus) and $Mn(NO_3)_2$ (Sinopharm Group) were used as precursors while silica gel (Qingdao Makall Group, BET surface area of 300 m^2/g) were used as a support. Generally, silica gel was first washed by 1.0 mol/L nitric acid, and then ground and sieved to desired granularity (20–40, 40–60, 60–80, 80–100 mesh) followed by washing with the ultra-pure water until neutral to remove any metal impurities. Finally, the silica gel was dried and calcined in an oven at 400 °C for 3 h before used as the catalyst support. Catalysts were prepared by co-impregnation to incipient wetness of the purified silica gel with the aqueous solution of $Rh(NO_3)_3$ and Mn $(NO_3)_2$ according to the calculated atomic ratios (1 mL solution per gram of silica gel). After the impregnation, mixtures were dried overnight at 100 °C and then calcined in an oven at 400 °C for 4 h with a ramping rate of 2 °C/min. All the catalysts were denoted as *x*Rh–*y*Mn, where *x* and *y* represent the weight fraction of each Rh and Mn, respectively. The loading amount of Rh was set at 1.5 wt% for comparison with the literatures (Gao et al., 2009a; Mo et al., 2009; Yu et al., 2012, 2013). The actual metal loading was measured by ICP–MS (Perkin-Elmer NexION 300).

2.2. Catalyst characterization

2.2.1. H_2 chemisorption

The dispersion of Rh particles was determined by H_2 chemisorption using a Micromeritics AutoChem II 2920 catalyst characterization system (USA). Prior to the measurement, ca. 0.1 g catalyst was degassed in an Ar flow (30 mL/min) at 120 °C for 2 h and then reduced at 350 °C in a H_2 flow (30 mL/min) for 2 h, followed by flushing with Ar (30 mL/min) at 380 °C for 2 h to remove any physically or chemically adsorbed impurities. After cooling down to 40 °C in the same Ar flow, H_2 uptake was measured by introducing pulses of H_2 with a quantitative loop into the Ar flow by a six-way valve. The pulses were continued until no further uptake of H_2 was detected. The amount of chemisorbed H_2 was obtained by extrapolating the total adsorption isotherm to zero pressure, and Rh dispersion (Rh_s/Rh_{total}) was calculated subsequently with assuming $H/Rh_s = 1$.

2.2.2. In situ diffuse reflectance infrared Fourier transform spectroscopy (DRIFTS)

A Perkin Elmer Spectrum 100 FTIR spectrometer equipped with a Harrick Praying Mantis cell was employed for the IR study. About 50 mg catalyst was ground and placed into the sample cup. Ultrahigh purity Ar, H_2 and CO (99.999%, Shanghai WOGE Gas Equipment Co., Ltd.) used in the DRIFTS study was purified by a de-oxygen trap and the flow rate were controlled by mass flow controllers. Prior to the experiment, the sample was reduced online at 350 °C under pure H_2 (30 mL/min) for 2 h, followed by Ar (30 mL/min) flushing at 350 °C for 1 h. Then, the background spectrum was taken at 270 °C. Afterwards $CO/H_2/Ar$ flow was introduced into the cell and the infrared spectra were taken at 4 cm^{-1} resolution at 270 °C. The flow rate and composition of the gas mixtures for CO/H_2 co-adsorption were 30 mL/min of 3.3%CO/6.6%H_2/Ar.

2.3. Kinetic measurement

Kinetic measurements were carried out in a continuous stainless steel fixed-bed micro-reactor with a length of 450 mm and an inner diameter of 5 mm, respectively. Three mass flow controllers were used to adjust automatically the flow rate of the inlet gases (H_2 (99.999%), N_2 (99.999%), and syngas with different CO/H_2 ratios, Shanghai WOGE Gas Equipment Co., Ltd.). After reaching the specified temperature through a preheater, the gas was introduced into the reactor, which was placed inside a tubular furnace. The reaction temperature was monitored by a K-type thermocouple inserted into the catalyst bed, which located in the middle of the reactor. A back pressure regulator was placed at the end of the pipeline to control the reaction pressure in the range 0.1–10.0 MPa. The conversion of CO was kept below 10.0% in order to ensure a differential condition. The external/internal diffusion effects were ruled out following the procedures introduced by previous studies (Madon and Boudart, 1982).

Prior to the reaction, the catalyst was first reduced in pure H_2 at 0.5 MPa, 350 °C for 2 h. Then, the catalyst was cooled down to the reaction temperature (270 °C) in the H_2 flow. The reaction was run in the mixed gas of $H_2/CO/N_2$ at a total pressure of 3.0 MPa with different CO, H_2 and N_2 partial pressures: 0.9 MPa H_2, 0.23–1.8 MPa CO, rest N_2; 0.54 MPa CO, 0.27–2.16 MPa H_2, rest N_2.

Before kinetic measurements, a blank test was done with 0.2 g purified SiO_2 sample. It could be inferred that less than 0.1%

conversion of CO was detected over SiO_2 (diluter) under reaction conditions (30% CO, 60% H_2 and 10% N_2, 3.0 MPa, GHSV of 3500 h^{-1}, 290 °C), indicating that the potential effects from the reactor wall and SiO_2 were excluded. In the meantime, the catalytic test for 1.0Mn/SiO_2 was also performed under the same reaction conditions. The result showed that 1.0Mn/SiO_2 was not active for CO hydrogenation, indicating that Mn only acted as a promoter in the catalysts.

Table 1
Rh and Mn compositions and morphologies of fresh reduced catalysts.

Catalysts	Rh (wt%)[a]	Mn (wt%)[a]	Atomic ratio of Mn/Rh[a]	Dispersion (%)[b]	Calculated particle size (nm)[c]
1.5Rh	1.4	0	0	64.2	1.8
1.5Rh–0.4Mn	1.5	0.4	0.5	74.3	1.5
1.5Rh–4.0Mn	1.5	3.9	5.0	65.8	1.7

[a] Based on ICP-mass analysis.
[b] Based on the irreversible chemisorption and assuming a stoichiometry of $H/Rh_s=1$.
[c] Calculated from H_2-chemisorption.

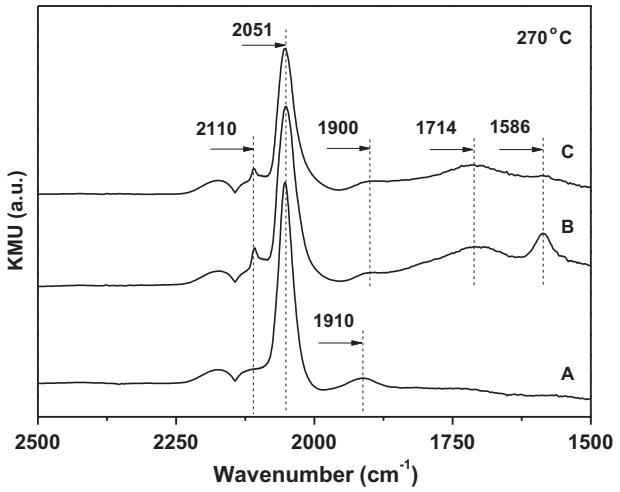

Fig. 1. DRIFTS spectra of CO/H_2 co-adsorption on Rh catalysts with different Mn loadings at 270 °C, 30 mL/min of CO/H_2/Ar. (A) 1.5Rh, (B) 1.5Rh–0.4Mn and (C) 1.5Rh–4.0Mn.

All the components in the effluent gas, including syngas, paraffins, olefins, carbon dioxide and oxygenated compounds (alcohols, acetaldehydes and acetic acid), were analyzed with an online gas chromatograph (Shanghai Ruimin GC2060) equipped with one thermal conductivity detector (TCD) and two flame ionization detectors (FID) using Ar as the carrier gas. A capillary column (HP-PLOT-Q) connected to one FID was used to analyze hydrocarbon products and oxygenated compounds. CO_2 was separated by a 6-foot long TDX-01 packed column and detected by the other FID through a methanation furnace at 360 °C. The unreacted syngas was determined using a 6-foot long 5A Molecular Sieve packed column connected to TCD. The oven temperature was held at 60 °C for 5 min and then ramped up to 220 °C at 10 °C/min, for 5 min. All the experimental data were obtained after reaction 16 h.

2.4. Calculations

The absolute reaction rate of CO hydrogenation (r_{CO}) is expressed as Eq. (1).

$$r_{CO} = \frac{v_{CO,in} \cdot X_{CO} \cdot Q_{in}}{m_{Rh}} \quad [mol/s/g_{Rh}] \tag{1}$$

m_{Rh} is the mass of Rh in the reactor bed; Q_{in} is the total molar flow rate; X_{CO} is the CO conversion based on the products formation; v_{CO} is the fraction of CO in the gas mixture, equal to p_i/p_0; p_i is the partial pressures of reactants; p_0 is the total pressure in the system.

Carbon monoxide conversion (X_{CO}) was determined from the summation of carbon numbers in all products (Eq. (2)).

$$X_{CO} = \frac{\Sigma n_i C_i}{n_{CO}} \times 100\% \tag{2}$$

The selectivity for each product was obtained by Eq. (3).

$$S_i = \frac{n_i C_i}{\Sigma n_i C_i} \times 100\% \tag{3}$$

Here CO conversion was kept less than ca. 10% to assure the differential condition. n_i and C_i are the carbon number and mole fraction of i component, respectively. n_{CO} is the mole fraction of CO in inlet gases.

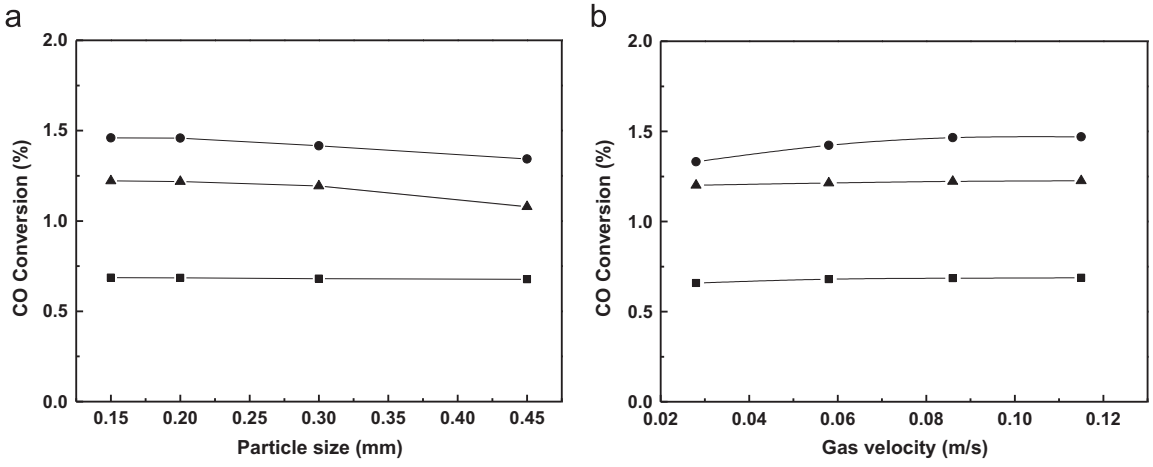

Fig. 2. (a) Dependence of CO conversion on different catalysts with a size of 0.42, 0.25, 0.18, and 0.15 mm, respectively, at 270 °C, 3.0 MPa, H_2:CO:N_2=6:3:1, GHSV: 15,000 h^{-1}. (-■- 1.5Rh, -●- 1.5Rh–0.4Mn, -▲- 1.5Rh–4.0Mn) and (b) Dependence of CO conversion on gas velocity of syngas over different catalysts (0.15 mm) at 270 °C, 3.0 MPa, H_2:CO:N_2=6:3:1. (-■- 1.5Rh, -●- 1.5Rh–0.4Mn, -▲- 1.5Rh–4.0Mn).

Space time yield (STY) of C_{2+} oxygenates were calculated through Eq. (4).

$$\mathrm{STY}(\mu g \cdot g_{cat}^{-1} \cdot s^{-1}) = \frac{\sum_{j=1}^{20} C_{ij} \cdot n_{total \cdot j} \cdot M_i}{m_{cat} t} \quad (4)$$

All data points were collected at each hour. C_{ij} is the mole fraction of the i component at the j hour. $n_{total\ j}$ is the total mole of the effluent gas at the j hour. M_i is the molar mass of i component. m_{cat} is the mass of the catalyst sample and t is the total reaction time (20 h).

The rate in TOF (r_{TOF}, s^{-1}) was calculated following Eq. (5)

$$r_{TOF} = \frac{r_{CO} M_{Rh}}{d_{Rh}} \times 100\% \quad [s^{-1}] \quad (5)$$

where M_{Rh}: atomic weight of Rh, d_{Rh}: dispersion of Rh. Here, we assume the surface Rh atoms to be main active sites. Dispersion of Rh atoms was calculated on the basis of a ball model.

Table 2
Effect of gas linear velocity on the external mass diffusion over Rh–MnO_x/SiO_2 catalysts.

Flow rate (mL/min)	Linear velocity (m/s)	k_c (m/s)
21.8	2.8×10^{-2}	3.3×10^{-2}
43.4	5.8×10^{-2}	3.4×10^{-2}
65.4	8.6×10^{-2}	3.5×10^{-2}
86.7	11.5×10^{-2}	3.5×10^{-2}

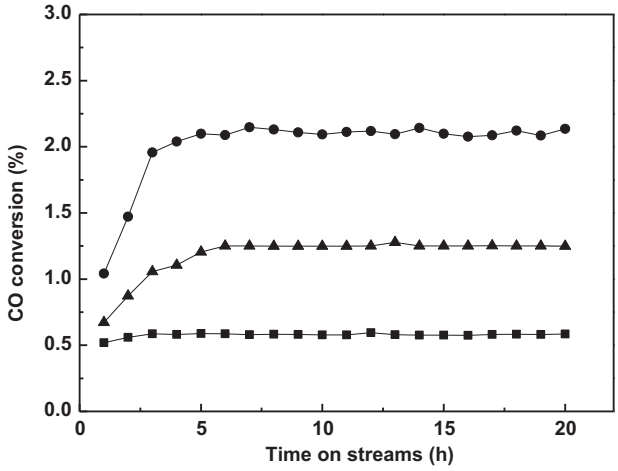

Fig. 3. Time-dependent reaction over Rh catalysts with different Mn loadings. Pretreatment: H_2 reduction for 2 h at 350 °C, 0.6 MPa; Reaction condition: H_2/CO=2, 270 °C, 3.0 MPa, GHSV=15,000 h^{-1}. (-■- 1.5Rh, -●- 1.5Rh–0.4Mn, -▲- 1.5Rh–4.0Mn).

3. Results and discussion

3.1. H_2-chemisorption

A series of Rh (1.5 wt%)–MnO_x catalysts were prepared with Mn contents of 0, 0.4 wt% and 4.0 wt%, corresponding to Mn/Rh atomic ratios of 0, 0.5 and 5.0, respectively. The dispersion of Rh atoms (Table 1) changed little according to the H_2 chemisorption, increasing slightly from 64.2% (1.5Rh) to 74.3% (1.5Rh–0.4Mn), but dropping to 65.8% for 4.0 wt% Mn.

3.2. DRIFTS studies for Surface structure of Rh at 270 °C

DRIFT spectra at 270 °C in CO/H_2/Ar are presented in Fig. 1. There are two types of adsorbed CO on the Rh/SiO_2 catalysts which centered at 2051 cm^{-1} and 1910 cm^{-1}, respectively. The band centered at 2051 cm^{-1}, which was 10 cm^{-1} lower than linear CO adsorption on Rh^0 under CO streams (Mo et al., 2009; Schwartz et al., 2011), might be ascribed to a carbonyl hydride species [H–Rh–CO] on Rh^0 (Solymosi et al., 1980; Yu et al., 2012). The electron donating from chemisorbed H to Rh and the increase in the π-donation from Rh to π anti-bonding orbital of CO leads to a decrease in CO stretching frequencies (Solymosi et al., 1980). On the other hand, the band at 1910 cm^{-1} might be ascribed to bridged CO adsorption on Rh^0 (Schwartz et al., 2011). These results indicate that both chain growth and CO insertion are preceded on both active sites. With the addition of MnO_x, three new bands appear at 2110, 1714 and 1586 cm^{-1}, respectively (Spectrum B and C in Fig. 1). The 2110 cm^{-1} band is ascribed to the linearly adsorbed CO on $Rh^{\delta+}$ sites, which plays an important role in the CO insertion step to produce oxygenates. Watson and Somorjai (1981) proposed that the CO insertion takes place on Rh oxide surfaces which could be important for the formation of ethanol and other oxygenates. The 1714 cm^{-1} band can be assigned to the tilted CO species on Rh–Mn interfaces, which can be ascribed to C bonded with Rh and O bonded Mn. It is generally accepted that this kind of CO species favors CO dissociation to form CH_x intermediates (Fukushima et al., 1985; Lisitsyn et al., 1990; Sachtler and Ichikawa, 1986). However, some studies indicated that tilted adsorbed CO species were inactive for the CO insertion during the reaction of C_2H_4/H_2 with pre-adsorbed CO on Rh–Ce/SiO_2 (Chuang et al., 1996) or Rh–Mn/SiO_2 (Chuang et al., 1997). Thus, those results indicate that the active sites on Rh surfaces altered indeed by MnO_x. The band at 1586 cm^{-1} might be ascribed to the surface formate species ($HCOO^-$), which agreed well with a stretching vibration at 1585 cm^{-1} detected after introducing HCOOH into Rh/Al_2O_3 catalysts (Solymosi et al., 1980). The surface formate species might be the intermediate for the formation of C_{2+} oxygenates, indicating that Mn-promoted Rh catalysts are more favorable for the formation of C_{2+} oxygenates than non-promoted Rh catalysts.

Table 3
Catalytic performance of Rh catalysts with different Mn loadings.[a]

Catalyst[a]	CO conv. (%)	Selectivity (%)[b]								
		CH_4	C_{2+} HCs[c]	MeOH	EtOH	PrOH	BuOH	AcH	AcOH	Total oxy.[d]
1.5Rh	0.8	64.1	11.7	6.8	8.5	1.1	0.5	3.6	2.7	16.4
1.5Rh–0.4Mn	1.6	39.8	12.5	7.9	19.9	1.1	0.6	9.6	5.0	38.2
1.5Rh–4.0Mn	1.2	44.7	12.6	6.4	19.7	1.2	0.6	7.3	3.9	34.7

[a] Catalyst: 0.1 g; pretreatment: 350 °C in H_2 flow at 0.5 MPa; reaction conditions: T=270 °C, P=3.0 MPa, GHSV=15,000 h^{-1} (30%CO, 60%H_2, 10%N_2). Data was recorded after reaching steady state. Error of ±10% of all the values measured.
[b] Carbon selectivity=$n_iC_i/\Sigma n_iC_i$.
[c] Hydrocarbons with two or more carbons.
[d] Including all C_{2+} oxygenates (alcohols, aldehyde, carboxylic acid and esters).

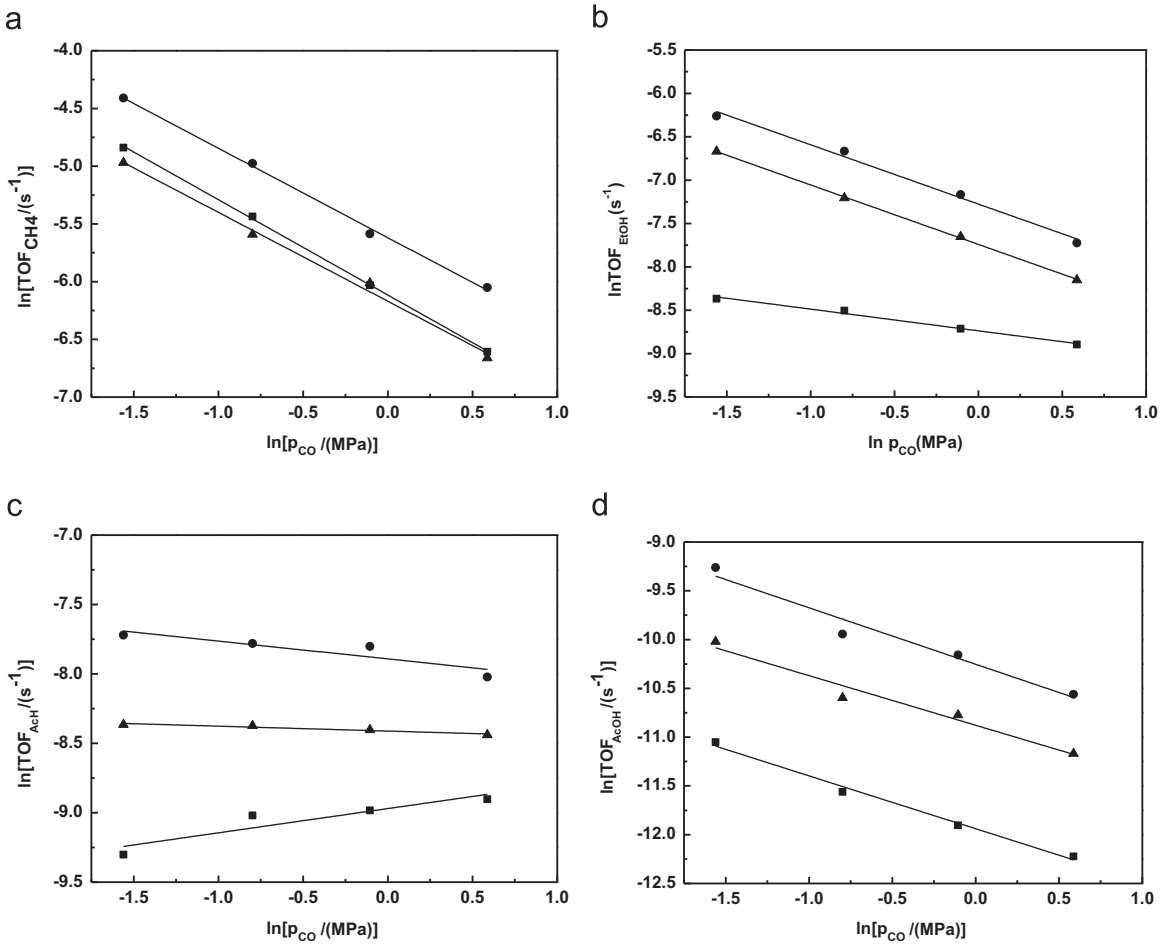

Fig. 4. Dependence of reaction rate of main products on partial pressure of CO over Rh catalysts with different Mn loadings. (-■- 1.5Rh, -●- 1.5Rh–0.4Mn, -▲- 1.5Rh–4.0Mn). (a) CH_4, (b) ethanol, (c) acetaldehyde and (d) acetic acid.

3.3. Kinetics of CO hydrogenation

3.3.1. Exclusion of the internal diffusion effects

Catalysts with different sizes were used to investigate the influence of the internal mass diffusion (Madon and Boudart, 1982). Fig. 2a showed the conversion of CO changed little with the variation of catalyst sizes below 0.3 mm. Therefore, the catalyst with an average size of 0.18 mm (80 mesh) was employed in the whole experiments to eliminate the influence of the internal mass diffusion.

3.3.2. Exclusion of the external diffusion effects

The catalyst with an average size of 0.15 mm was used to study the influence of the external mass diffusion. The amount of the catalyst sample and flow rate of the gas stream were varied to change the gas linear velocity through the catalyst bed with a GHSV of 15,000 h^{-1} (Madon and Boudart, 1982). Fig. 2b shows the changes in CO conversions with different gas velocities at the steady state. CO conversion reached a constant at the gas velocity through the bed above 0.086 m/s, which means that the external mass diffusion can be excluded.

The Frossling correlation is generally used to evaluate the external mass diffusion in catalysis, especially in flow around spherical particles to obtain the relations among the particle size (d_p) of the catalyst, mass-transfer coefficient (k_c) and boundary layer thickness (δ). The mass-transfer correlation is given as Eq. (6):

$$Sh = 2 + 0.6Re^{1/2}Sc^{1/3}, \quad Sh = \frac{k_c d_p}{D_e}, \quad Re = \frac{\rho u d_p}{\mu}, \quad \text{and} \quad Sc = \frac{\mu}{\rho D_e} \tag{6}$$

here k_c is the average mass-transfer coefficient of a reactant from the bulk flow to catalyst surface (m/s), d_p is the average diameter of the catalyst particle (m), D_e is the effective diffusivity for a binary gas mixture (m^2/s), u is the free stream velocity of fluid (m/s), ρ is the gas density (kg/m^3), and μ is the gas dynamic viscosity (kg/m/s). The average mass-transfer coefficient k_c corresponding to the linear velocity is listed in Table 2. The results show that the external mass diffusion could be ruled out at the linear velocity above 0.086 m/s, which coincides with the experimental results.

3.3.3. Catalyst stability and catalytic performance

All catalysts (1.5Rh, 1.5Rh–0.4Mn, 1.5Rh–4.0Mn) showed good stabilities after 20 h time-on-stream under 270 °C, 3.0 MPa (Fig. 3). The results indicate that the structure of active sites for the formation of C_{2+} oxygenates was unlikely altered during the reaction.

The catalytic performance of CO hydrogenation over Rh–MnO_x catalysts with different Mn loadings after eliminating internal and external diffusion at the typical reaction conditions (270 °C, 3.0 MPa) is listed in Table 3. It can be seen that the conversion of CO and selectivity of C_{2+} oxygenates were enhanced by the addition of MnO_x while the formation of methane was suppressed.

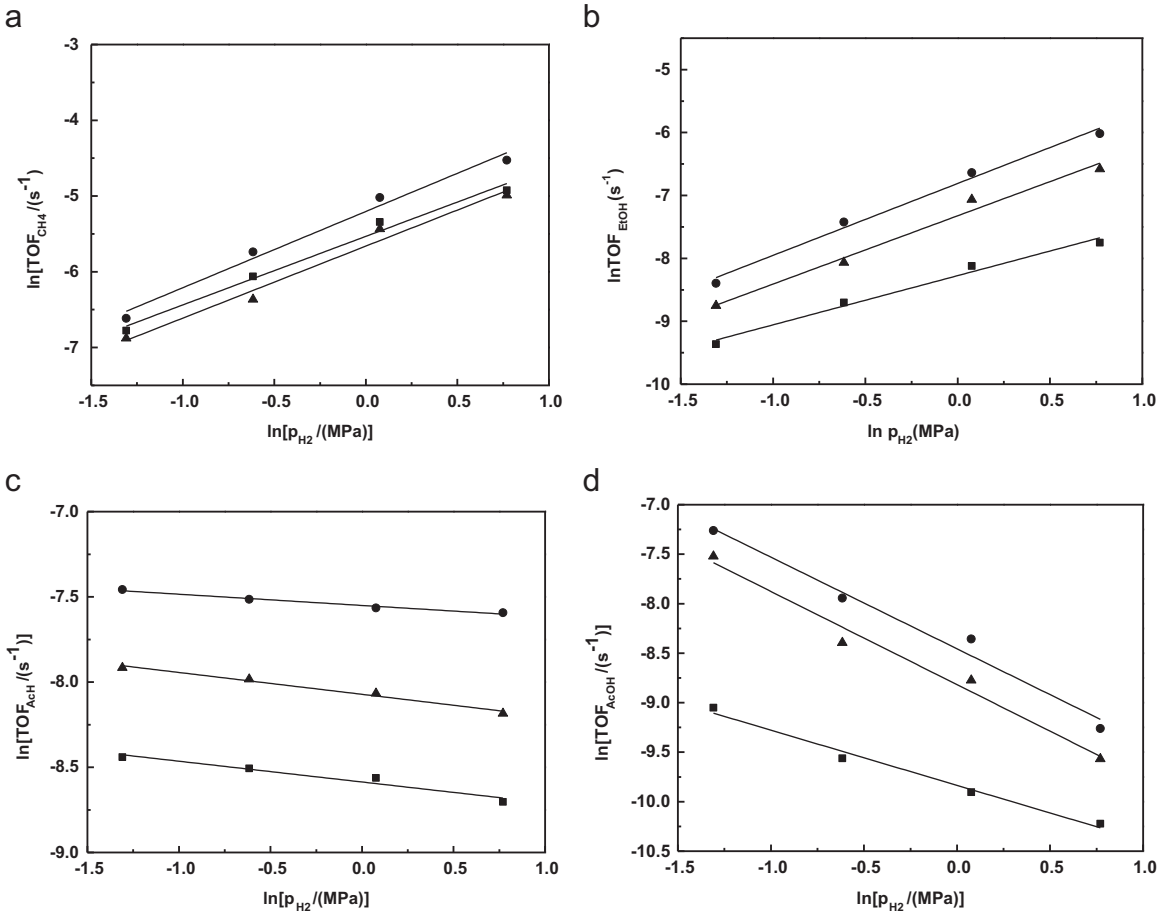

Fig. 5. Dependence of reaction rate of main products on partial pressure of H_2 over Rh catalysts with different Mn loadings. (-■- 1.5Rh, -●- 1.5Rh–0.4Mn, -▲- 1.5Rh–4.0Mn). (a) CH_4, (b) ethanol, (c) acetaldehyde and (d) acetic acid.

Table 4
Apparent kinetic parameters[a,b] of hydrocarbons on Rh based catalysts with different Mn loadings at 270 °C and 3.0 MPa.

Product	1.5Rh			1.5Rh–0.4Mn			1.5Rh–4.0Mn		
	E_a (kJ/mol)	x	y	E_a (kJ/mol)	x	y	E_a (kJ/mol)	x	y
CH_4	87.2 ± 1.1	−0.8 ± 0.01	0.9 ± 0.07	121.9 ± 7.7	−0.8 ± 0.02	1.0 ± 0.09	119.6 ± 5.5	−0.8 ± 0.04	1.0 ± 0.09
C_2H_4	71.5 ± 4.1	1.1 ± 0.04	−0.5 ± 0.02	90.4 ± 2.2	1.1 ± 0.07	−0.5 ± 0.03	84.3 ± 4.8	1.1 ± 0.04	−0.5 ± 0.02
C_2H_6	84.4 ± 2.2	−0.5 ± 0.03	0.9 ± 0.08	108.8 ± 3.4	−0.2 ± 0.01	1.0 ± 0.07	113.0 ± 2.4	−0.3 ± 0.03	1.0 ± 0.07
C_3H_6	64.6 ± 4.2	0.7 ± 0.06	−0.6 ± 0.03	74.6 ± 4.3	0.4 ± 0.06	−0.5 ± 0.14	72.5 ± 2.6	0.3 ± 0.04	−0.5 ± 0.01
C_3H_8	82.6 ± 4.4	−0.6 ± 0.02	1.0 ± 0.04	96.1 ± 5.0	−0.5 ± 0.02	1.0 ± 0.02	94.1 ± 4.1	−0.5 ± 0.06	1.0 ± 0.04
C_4H_8	36.4 ± 6.2	0.9 ± 0.09	−0.5 ± 0.04	52.7 ± 7.7	0.9 ± 0.07	−0.5 ± 0.05	52.2 ± 7.3	0.8 ± 0.06	−0.5 ± 0.05
C_4H_{10}	53.6 ± 2.1	−0.3 ± 0.02	1.0 ± 0.03	73.3 ± 2.8	−0.2 ± 0.02	1.0 ± 0.04	71.8 ± 2.2	−0.3 ± 0.02	1.1 ± 0.03

[a] The reaction orders of CO and H_2 were determined by fitting a power-law rate expression as Eq. (7).
[b] Apparent activation energies (E_a) of reactant CO and products were determined by Arrhenius equation as Eq. (8).

3.4. Effect of MnO_x on kinetics

By kinetic measurements, the power-law function was employed for fitting the kinetic data. The reaction rate for the formation of each product i can be expressed as Eq. (7). The parameters include apparent activation energies (E_a) and reaction orders with respect to CO (x) and H_2 (y), which can reflect the effects of reaction temperature and reactant partial pressures directly on the rate. In addition, the simple model also has an important guiding significance for the scaling-up of reactor.

$$r_i = k \cdot p_{CO}^{x} \cdot p_{H_2}^{y} \tag{7}$$

where the rate constant k can be expressed as Eq. (8):

$$k = k_0 \cdot e^{-\frac{E_a}{RT}} \tag{8}$$

The dependence of reaction rates with respect to H_2 partial pressure (p_{CO}=0.54 MPa, p_{H_2}=0.27–2.16 MPa) and CO partial pressure (p_{H_2}=0.9 MPa, p_{CO}=0.23–1.8 MPa) of main products (methane, ethanol, acetaldehyde and acetic acid) and by products (methanol, C_{2+} hydrocarbons and oxygenates) at 270 °C are depicted in Figs. 4 and 5 and S1–S2, respectively. All the reaction orders with respect to CO and H_2 over Rh catalysts with different

Table 5
Apparent kinetic parameters[a,b] of oxygenates and CO_2 calculated on the basis of the transformation of CO on Rh based catalysts with different Mn loadings at 270 °C and 3.0 MPa.

Product	1.5Rh			1.5Rh–0.4Mn			1.5Rh–4.0Mn		
	E_a (kJ/mol)	x	y	E_a (kJ/mol)	x	y	E_a (kJ/mol)	x	y
MeOH	52.5 ± 3.3	0.1 ± 0.01	2.0 ± 0.12	57.0 ± 2.7	-0.1 ± 0.01	1.9 ± 0.16	55.6 ± 2.0	-0.1 ± 0.02	1.9 ± 0.10
EtOH	84.3 ± 3.7	-0.3 ± 0.02	0.8 ± 0.07	91.0 ± 3.0	-0.7 ± 0.04	1.1 ± 0.08	89.9 ± 3.7	-0.7 ± 0.01	1.1 ± 0.10
AcH	85.2 ± 5.0	0.2 ± 0.05	-0.1 ± 0.02	89.6 ± 3.5	-0.1 ± 0.04	-0.1 ± 0.01	88.1 ± 2.8	-0.1 ± 0.01	-0.1 ± 0.01
AcOH	74.2 ± 4.7	-0.5 ± 0.04	-0.6 ± 0.05	75.6 ± 2.7	-0.6 ± 0.08	-0.9 ± 0.09	76.7 ± 2.3	-0.5 ± 0.07	-0.9 ± 0.09
PrOH	76.8 ± 3.5	0.4 ± 0.02	0.6 ± 0.06	79.1 ± 2.4	0.1 ± 0.03	0.7 ± 0.05	79.4 ± 3.1	0.1 ± 0.01	0.7 ± 0.07
BuOH	87.0 ± 6.0	0.5 ± 0.04	0.7 ± 0.11	94.5 ± 5.9	0.4 ± 0.03	0.8 ± 0.06	94.3 ± 5.6	0.4 ± 0.02	0.7 ± 0.08
CO_2	93.3 ± 9.0	0.1 ± 0.02	/	91.9 ± 7.7	-0.3 ± 0.02	/	95.3 ± 7.5	-0.1 ± 0.01	/

[a] The reaction orders of CO and H_2 were determined by fitting a power-law rate expression as Eq. (7).
[b] Apparent activation energies (E_a) of reactant CO and products determined by Arrhenius equation as Eq. (8).

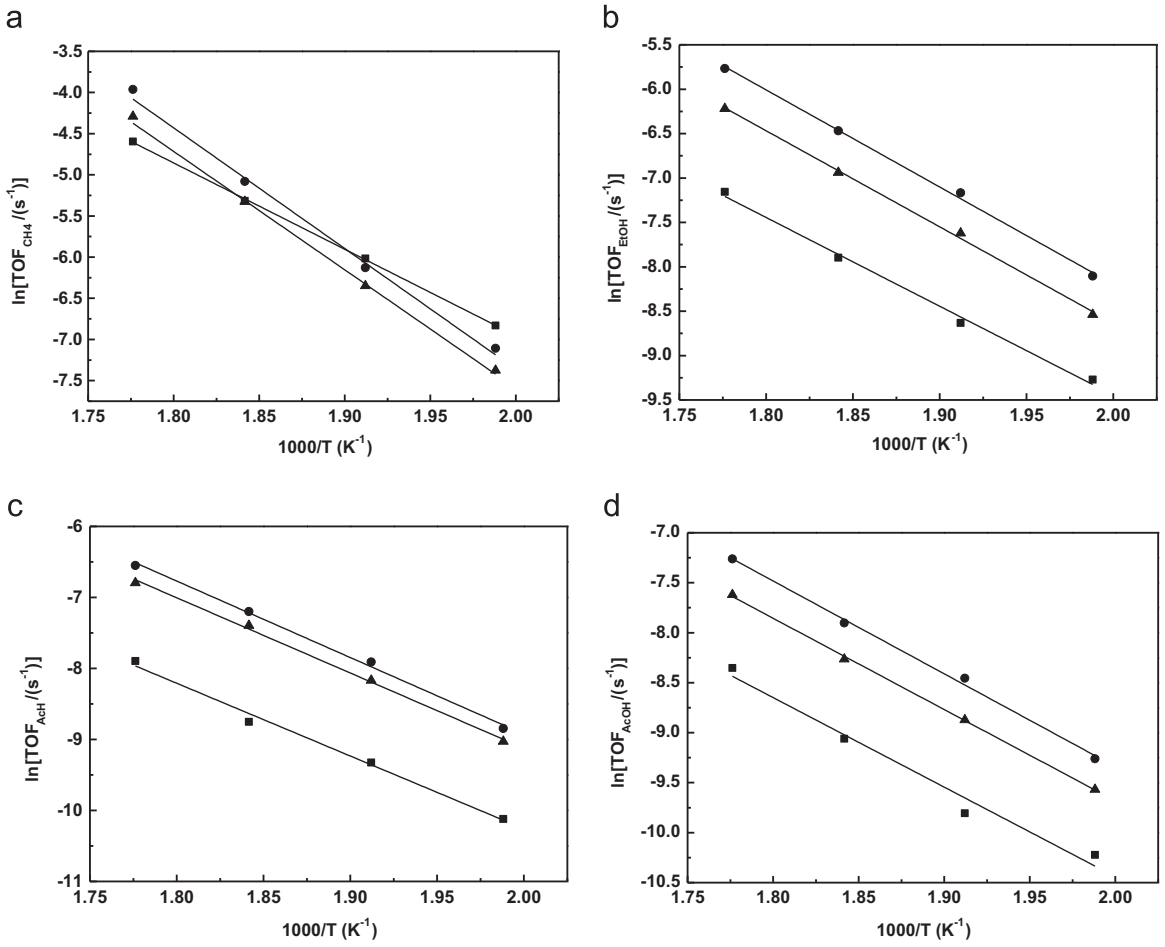

Fig. 6. Arrhenius plots of main products over Rh catalysts with different Mn loadings. (-■- 1.5Rh, -●- 1.5Rh–0.4Mn, -▲- 1.5Rh–4.0Mn). (a) methane, (b) ethanol, (c) acetaldehyde and (d) acetic acid.

Mn loadings and E_a were calculated on the basis of yields for different products after linear fittings of the data (Tables 4 and 5). The dependence of reaction rates based on the formation of main products and by products on the reciprocal of the reaction temperature at 230–290 °C (the Arrhenius plots) is presented in Figs. 6 and S3, respectively.

3.4.1. *Effect of MnO_x on E_a*

From Tables 4 and 5, the E_a for the formation of hydrocarbons differs slightly with that of oxygenates over Rh/SiO_2. However, after loading 0.4 wt% Mn, the E_a of hydrocarbons increases significantly (e.g. 87.2 kJ/mol to 121.9 kJ/mol for methane, and 84.4 kJ/mol to 108.8 kJ/mol for ethane) while the E_a for oxygenates increases slightly (e.g. 84.3 kJ/mol to 91.0 kJ/mol for EtOH, and 85.2 kJ/mol to 89.6 kJ/mol for AcH). The fact demonstrates that the formation of hydrocarbons could be kinetically suppressed by MnO_x, which was similar to that reported by Choi and Liu (2009) via micro-kinetic modeling. They have evidenced that the addition of Fe promoter could dramatically increase the barrier of methane formation. Moreover, those reaction orders calculated on the same product varied little with an increase in the Mn content, indicating

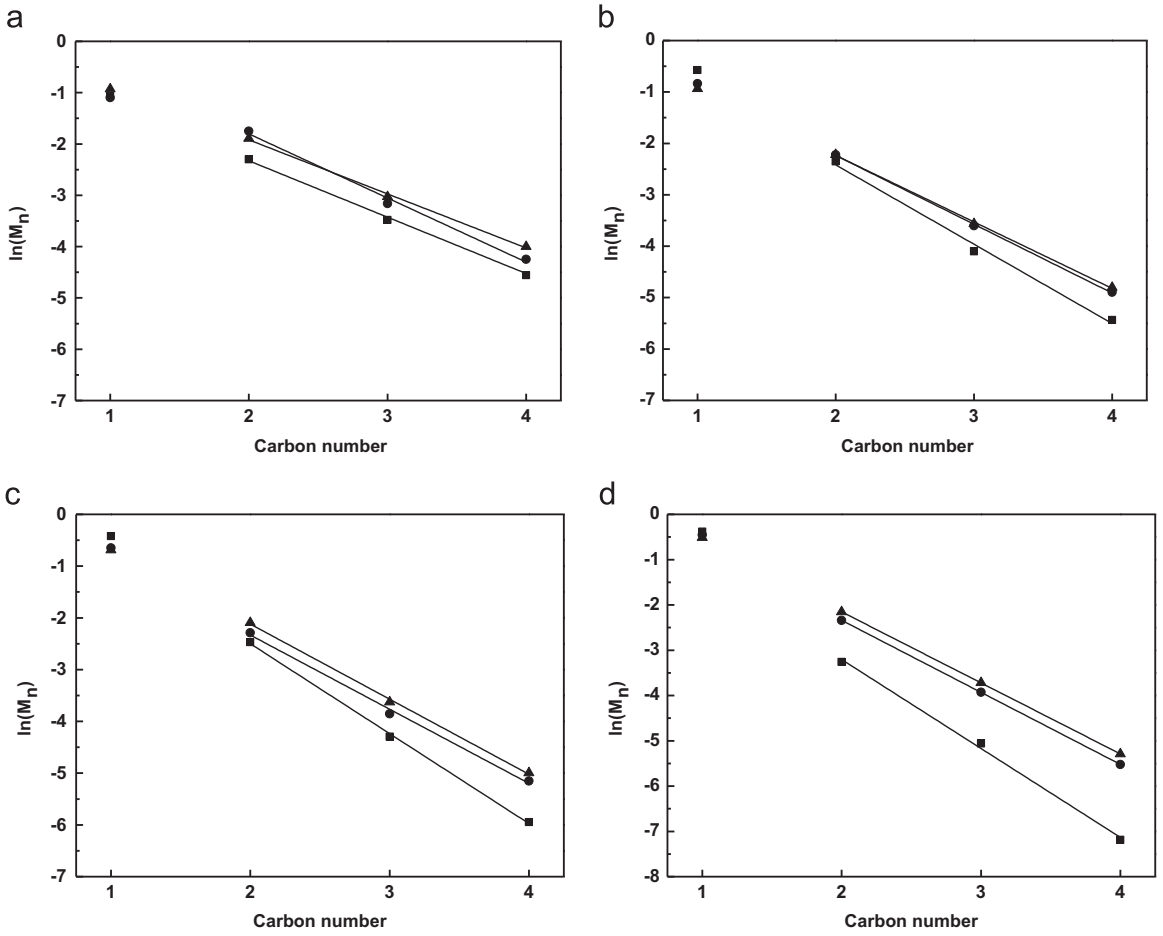

Fig. 7. ASF fitting for hydrocarbons over Rh catalysts with different Mn loadings at (a) 230 °C, (b) 250 °C, (c) 270 °C and (d) 290 °C. Reaction conditions: 3.0 MPa, H_2:CO: N_2=6:3:1 and GHSV=15,000 h^{-1}. (-■- 1.5Rh, -●- 1.5Rh–0.4Mn, -▲- 1.5Rh–4.0Mn).

that the active sites for C_{2+} oxygenates were kept constant regardless of excessive addition of Mn.

3.4.2. *Effect of MnO_x on reaction orders of products*

The power-law rate functions in the form of $r_i = k_0 e^{-E_a/RT} p_{CO}^x p_{H_2}^y$ for the synthesis of hydrocarbons and oxygenates (alcohols, aldehydes, carboxylic acids) are summarized in Tables 4 and 5. Since the formation of different products from CO hydrogenation follows somewhat different pathways, it is more meaningful to examine the power-law rate parameters for the individual product rather than the rate parameters for the overall reaction of CO. The low standard deviations for E_a and reaction order measurements along with their correlation coefficients (>0.95) indicate that these parameters represent the data well. In this study, the effects of MnO_x on kinetics over Rh catalysts are mainly discussed. Compared with the pure Rh catalyst, CO and H_2 orders of all hydrocarbons remained unchanged with the addition of MnO_x, indicating that the formation mechanism of hydrocarbons was little affected. However, with the addition of MnO_x, CO order of ethanol dropped to about -0.7 from -0.3 while H_2 order of ethanol increased to about 1.1 from 0.8. That means the coverage of surface C* intermediates or non-dissociatively adsorbed CO on Rh sites can be enhanced. In accordance to the mechanism as proposed in our previous work, CO orders of hydrocarbons would be reduced with an increase in the coverage of C* species; however, this phenomenon was not observed in Table 4. In other words, the addition of MnO_x enhanced the coverage of non-dissociatively adsorbed CO, which was partially proved by CO-DRIFTS, thus CO orders decreased with the rise of the amount of CH_3CO^* species. Similarly, the enhancement of H_2 coverage improved the yield of EtOH via hydrogenation of CH_3CO^* species. But the H_2 orders of AcOH dropped to -0.9 from -0.6, caused by the competition among hydrogenation of CH_3CO^*, hydrogenation of OH* and OH* insertion to CH_3CO^* species.

3.5. *ASF distribution*

Chain growth is a key step in C_{2+} oxygenates synthesis, and the distribution of oxygenates could be described by Anderson–Schulz–Flory distribution (Eq. (9)) as it is widely used in F–T synthesis.

$$\ln\left(\frac{W_n}{n}\right) = n \cdot \ln\alpha + 2\ln\left(\frac{1-\alpha}{\sqrt{\alpha}}\right) \tag{9}$$

The ASF product distribution for the formation of oxygenates and hydrocarbons at different temperatures are shown in Figs. 7 and 8. It is noted that C_1 products such as methanol and methane were plotted but not included in the chain growth probability calculations because Rh catalysts are not typical Fischer–Tropsch catalysts as Fe or Co based catalysts. That is to say, C_1 products are not generated from chain growth steps but only hydrogenation of dissociated C* species or non-dissociated CO* species. The oxygenate distribution shows less C_1 (methanol) than would be expected by extrapolation of the ASF distribution for C_{2+} oxygenates according to the distribution of oxygenates, suggesting that the pathway for methanol formation is different from that for ethanol and other higher oxygenates. As mentioned

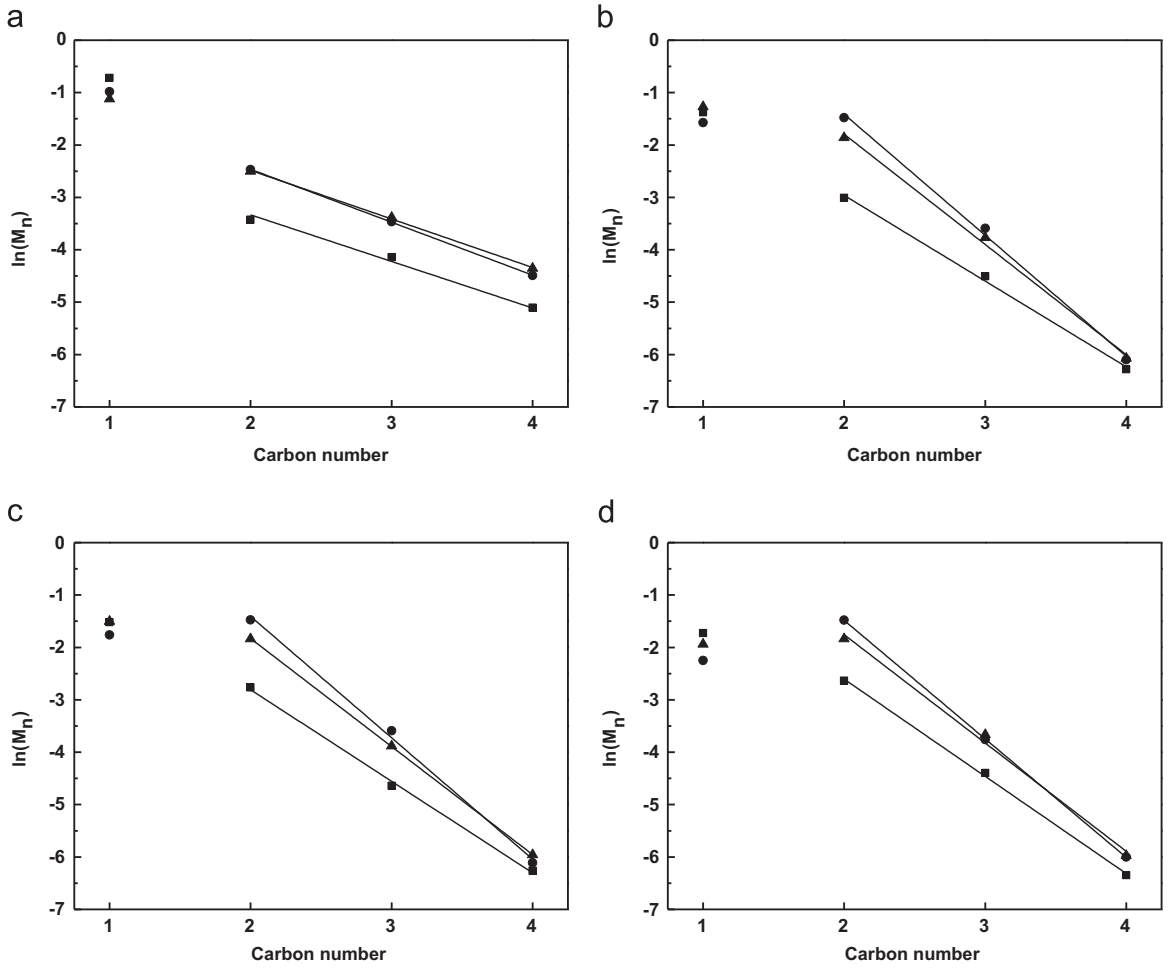

Fig. 8. ASF fitting for oxygenates over Rh catalysts with different Mn loadings at (a) 230 °C, (b) 250 °C, (c) 270 °C and (d) 290 °C. Reaction conditions: 3.0 MPa, H_2:CO: N_2=6:3:1 and GHSV=15,000 h^{-1}. (-■- 1.5Rh, -●- 1.5Rh–0.4Mn, -▲- 1.5Rh–4.0Mn).

above, methanol is presumably formed by direct hydrogenation of non-dissociated CO* rather than chain growth after CO dissociation as C_{2+} oxygenates. Thus the formation of methanol does not follow the chain growth mechanism. On the contrary, the hydrocarbon distribution shows that the amount of methane is more than expected based on the distribution of C_{2+} hydrocarbons. This suggests that only a part of the surface hydrocarbon species, $(CH_x)_{ads}$, resulting from the hydrogenation of the surface carbon formed in CO dissociation, participates in the ASF chain growth mechanism to form C_{2+} hydrocarbons. Most of CH_x species undergo further hydrogenation to form methane. In other words, methane is also formed by a mechanism without chain growth. Furthermore, the distributions for C_{2+} hydrocarbon and oxygenate products comply with the ASF distribution, but the chain growth probabilities vary with different Mn loadings (Table 6).

For Rh/SiO_2, the chain growth probabilities for hydrocarbons and oxygenates are very close, indicating those products are formed over the same active sites. With the addition of MnO_x, the chain growth probability of hydrocarbons changed little, in contrast, the chain growth probability of oxygenates decreased dramatically. Those results suggest that the reactions leading to these products may either proceed by diverse mechanisms or on different active sites. For Rh/SiO_2, both chain growth and CO insertion steps occur on Rh^0 active sites (linear or bridged CO), resulting in similar chain growth probabilities of hydrocarbons and oxygenates. The surface of Rh–MnO_x is much more complex than the Rh alone. Chain growth and CO insertion steps may take place on different active sties, which are responsible for the variation of chain growth probabilities for hydrocarbons and oxygenates.

3.6. *Promotional effects of MnO_x*

The catalytic performance of Rh/SiO_2 was greatly enhanced with the addition of MnO_x. Kinetic behaviors and product distributions have been investigated on Rh–MnO_x catalysts with different compositions. Therefore, in this section, the discussion is focused on two aspects: (i) the MnO_x structural modification by the interaction with Rh, and its effects on the catalyst performance; (ii) the plausible mechanism for CO hydrogenation on the basis of kinetics. It is noted that Rh is regarded as the primary active metal in this system. However, the conversion of syngas over the Rh alone will not be mentioned in detail here, because it has already been studied widely.

The mechanism for the formation of methane addressed here will enlighten us to understand the effect of promoters on CO hydrogenation. However, even for methane formation, there are disagreements in the literature about whether C–O bond cleavage occurs in CO hydrogenation via direct dissociation (carbide models) or via a hydrogen-enhanced process. There has been an increasing focus more recently on the latter mechanism because several studies have provided strong evidences supporting this mechanism over Rh catalysts (Davis, 2001; Fisher and Bell, 1996; Storsæter et al., 2006; Su et al., 2014).

It is well known that Rh catalysts have been attracting to industry in selective CO hydrogenation, which is a surface-catalyzed polymerization process. CH_x monomers, yielded by the hydrogen-assisted

Table 6
Chain growth probability of Rh catalyst with different Mn loadings.

Sample	230 °C		250 °C		270 °C		290 °C	
	HCs	oxy	HCs	oxy	HCs	oxy	HCs	oxy
1.5Rh	0.41	0.33	0.21	0.20	0.18	0.17	0.14	0.16
1.5Rh–0.4Mn	0.36	0.29	0.26	0.10	0.24	0.10	0.20	0.10
1.5Rh–4.0Mn	0.40	0.35	0.27	0.12	0.23	0.13	0.21	0.13

activation of adsorbed CO, are the building blocks for the subsequent chain growth reactions to produce paraffins, olefins, alcohols and oxygenates. The well-accepted pathway for syngas conversion was illustrated in Scheme 1 (Chuang et al., 2005), which includes several primary steps, such as CO dissociation, *C hydrogenation and CO insertion into $*CH_x$.

The reaction rate and selectivity to C_{2+} oxygenates over Rh catalysts were affected by several factors, such as the size of Rh crystallites (Arakawa et al., 1984; Kapur et al., 2010), the support property (Sachtler and Ichikawa, 1986), the Rh–RhO_x assemble and the second metal (Ojeda et al., 2004). In this study, we only discuss the production of C_{2+} oxygenates affected by MnO_x and the role of $Rh^{\delta+}$ because the particle size of Rh changed slightly in the range of 1.5–1.8 nm after the addition of Mn. Hence, we proposed the enhancement of selectivity to C_{2+} oxygenates may be caused by the modification of Rh electronic structure rather than the particle size of Rh after addition of Mn. With the combination of the DRIFTS spectra (Fig. 1) and kinetic parameters (Tables 3–5), it can be seen that CO conversion and selectivities of C_{2+} oxygenates were greatly enhanced by linearly adsorbed CO species on $Rh^{\delta+}$ sites and tilted species on Rh–MnO_x sites.

The reaction pathways over Rh and Rh–MnO_x were illustrated in Scheme 1. The reaction pathway for the former is marked as the straight line while both straight line and dashed line are marked for the latter. For Rh catalysts, all the elementary steps (CO dissociation, chain growth, hydrogenation and CO insertion) take place on metallic Rh^0 surfaces (Chuang et al., 2005; Egbebi and Spivey, 2008). For Rh–MnO_x catalysts, CO dissociation and chain growth steps take place on metallic Rh^0 and the presence of MnO_x could enhance CO dissociation through the production of a titled CO adsorbed at the Rh–MnO_x interface (Sachtler and Ichikawa, 1986; Wang et al., 2000). On the other hand, CO insertion, the key step for the formation of oxygenates, is highly active on $Rh^{\delta+}$ sites after the addition of MnO_x. Watson and Somorjai (1981) also proposed that RhO_x played an important role in the formation of C_{2+} oxygenates from CO hydrogenation over Rh catalysts. In the meantime, the ASF distribution in Table 6 shows the chain growth probability for C_{2+} oxygenates decreased rapidly in the presence of MnO_x. This fact indicates that CH_2CO^* species on $Rh^{\delta+}$ sites selectively favor the formation of oxygenates after hydrogenation rather than chain growth to form $C_2H_4CO^*$. On the contrary, CH_2CO^* on Rh^0 sites can either go through hydrogenation to form oxygenates or chain growth to yield long chain oxygenates. Thus, it can be concluded that MnO_x in Rh–MnO_x can enhance CO insertion pathways that form oxygenates while the hydrogenation of $*CH_x$ and chain growth reaction by inserting $*CH_x$ are significantly depressed (Scheme 1).

As a summary, we have demonstrated that the structure of Rh particles could be modified upon interacting with MnO_x and varied with the change in Mn loadings. Consequently, the activity and selectivity to C_{2+} oxygenates over Rh–MnO_x catalysts were improved significantly. In the studied system, the morphology and size of Rh particles play trivial roles in this reaction. Nevertheless, the fine structure of the surface species, such as Rh–MnO_x, Rh–O–Mn or Rh–RhO_x, which may impact on selective hydrogenation of C_{2+} oxygenates, need to be further identified for both understanding the mechanisms and redesigning catalysts with higher efficiencies.

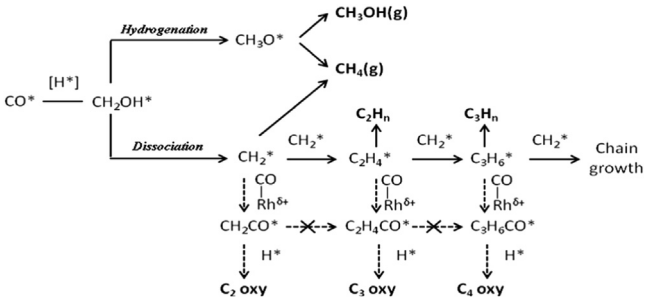

Scheme 1. Pathways for the formation of methane, methanol and C_{2+} oxygenates from CO hydrogenation over Rh–MnO_x/SiO_2 catalysts. (Reactions of dashed arrows took place only over Mn promoted Rh/SiO_2 catalysts).

4. Conclusions

The mechanistic basis of the effects of MnO_x loading on syngas to C_{2+} oxygenates were studied over Rh–MnO_x/SiO_2 catalysts with different Mn/Rh molar ratios (0, 0.5 and 5). The kinetic parameters of CO hydrogenation over the three catalysts at 270 °C, 3.0 MPa were obtained using a power law model. It was found that apparent activation energies changed slightly for the formation of oxygenates but increased rapidly for the formation of hydrocarbons when promoted by MnO_x. DRIFTS study at 270 °C under $CO/H_2/Ar$ flow indicates that there appear two new active sites over Rh–MnO_x/SiO_2 catalysts, which may play an important role in CO dissociation and CO insertion. The reaction orders with respect to CO are negative and positive value to H_2 orders for all paraffins; totally opposite results were obtained for all olefins. C_{2+} oxygenates have been assumed to be formed via non-dissociated CO insertion and further hydrogenation of CH_2CO^* species.

Acknowledgment

The authors are grateful to the support from the National Science Foundation (21176071, 21106041, 21273070), the Program for New Century Excellent Talents in University (NCET-12-0852), Science and Technology Commission of Shanghai Municipality (11JC1402700), International Cooperation Project of Shanghai Ministry of Science and Technology (14230710700) and the Chinese Education Ministry 111 project (B08021).

Appendix A. Supporting information

Supplementary data associated with this article can be found in the online version at http://dx.doi.org/10.1016/j.ces.2015.03.023.

References

Arakawa, H., Takeuchi, K., Matsuzaki, T., Sugi, Y., 1984. Effect of metal dispersion on the activity and selectivity of Rh/SiO_2 catalyst for high pressure CO hydrogenation. Chem. Lett. 13, 1607–1610.
Bhasin, M.M., Bartley, W.J., Ellgen, P.C., Wilson, T.P., 1978. Synthesis gas conversion over supported rhodium and rhodium-iron catalysts. J. Catal. 54, 120–128.
Chen, W., Ding, Y., Song, X., Wang, T., Luo, H., 2011. Promotion effect of support calcination on ethanol production from CO hydrogenation over $Rh/Fe/Al_2O_3$ catalysts. Appl. Catal., A: Gen. 407, 231–237.
Choi, Y., Liu, P., 2009. Mechanism of ethanol synthesis from syngas on Rh(1 1 1). J. Am. Chem. Soc. 131, 13054–13061.
Chuang, S.S.C., Brundage, M.A., Balakos, M.W., 1997. Mechanistic study in catalysis using dynamic and isotopic transient infrared spectroscopy: $CO/H_2/C_2H_4$ reaction on $MnRh/SiO_2$. Appl. Catal., A: Gen. 151, 333–354.

Chuang, S.S.C., Srinivas, G., Brundage, M.A., 1996. Role of tilted CO in dynamics of CO insertion on Ce–Rh/SiO_2. Energy Fuels 10, 524–530.
Chuang, S.S.C., Stevens, R.W., Khatri, R., 2005. Mechanism of C_{2+} oxygenate synthesis on Rh catalysts. Top. Catal. 32, 225–232.
Davis, B.H., 2001. Fischer–Tropsch synthesis: current mechanism and futuristic needs. Fuel Process. Technol. 71, 157–166.
Egbebi, A., Spivey, J.J., 2008. Effect of H_2/CO ratio and temperature on methane selectivity in the synthesis of ethanol on Rh-based catalysts. Catal. Commun. 9, 2308–2311.
Farrell, A.E., Plevin, R.J., Turner, B.T., Jones, A.D., O'Hare, M., Kammen, D.M., 2006. Ethanol can contribute to energy and environmental goals. Science 311, 506–508.
Fisher, I.A., Bell, A.T., 1996. A comparative study of CO and CO_2 hydrogenation over Rh/SiO_2. J. Catal. 162, 54–65.
Fukushima, T., Arakawa, H., Ichikawa, M., 1985. High-pressure I.R. spectroscopic evidence of acetyl and acetate species directly formed in CO–H_2 conversion on SiO_2-supported Rh and Rh–Mn catalysts. J. Chem. Soc., Chem. Commun., 729–731.
Gao, J., Mo, X., Chien, A.C.-Y., Torres, W., Goodwin Jr, J.G., 2009a. CO hydrogenation on lanthana and vanadia doubly promoted Rh/SiO_2 catalysts. J. Catal. 262, 119–126.
Gao, J., Mo, X., Goodwin Jr, J.G., 2009b. La, V, and Fe promotion of Rh/SiO_2 for CO hydrogenation: detailed analysis of kinetics and mechanism. J. Catal. 268, 142–149.
Kapur, N., Hyun, J., Shan, B., Nicholas, J.B., Cho, K., 2010. Ab initio study of CO hydrogenation to oxygenates on reduced Rh terraces and stepped surfaces. J. Phys. Chem. C 114, 10171–10182.
Lisitsyn, A.S., Stevenson, S.A., Knözinger, H., 1990. Carbon monoxide hydrogenation on supported Rh–Mn catalysts. J. Mol. Catal. 63, 201–211.
Ma, X.F., Su, H.Y., Deng, H.Q., Li, W.X., 2011. Carbon monoxide adsorption and dissociation on Mn-decorated Rh(1 1 1) and Rh(5 5 3) surfaces: a first-principles study. Catal. Today 160, 228–233.
Madon, R.J., Boudart, M., 1982. Experimental criterion for the absence of artifacts in the measurement of rates of heterogeneous catalytic reactions. Ind. Eng. Chem. Fundam. 21, 438–447.
McClure, S.M., Lundwall, M.J., Goodman, D.W., 2011. Planar oxide supported rhodium nanoparticles as model catalysts. Proc. Natl. Acad. Sci. U.S.A. 108, 931–936.
Mo, X., Gao, J., Goodwin Jr, J.G., 2009. Role of promoters on Rh/SiO_2 in CO hydrogenation: a comparison using DRIFTS. Catal. Today 147, 139–149.
Ojeda, M., Granados, M.L., Rojas, S., Terreros, P., Garcia-Garcia, F.J., Fierro, J.L.G., 2004. Manganese-promoted Rh/Al_2O_3 for C_2-oxygenates synthesis from syngas —effect of manganese loading. Appl. Catal., A: Gen. 261, 47–55.
Sachtler, W.M.H., Ichikawa, M., 1986. Catalytic site requirements for elementary steps in syngas conversion to oxygenates over promoted rhodium. J. Phys. Chem. 90, 4752–4758.
Schwartz, V., Campos, A., Egbebi, A., Spivey, J.J., Overbury, S.H., 2011. EXAFS and FT-IR characterization of Mn and Li promoted titania-supported Rh catalysts for CO hydrogenation. ACS Catal. 1, 1298–1306.
Solymosi, F., Erdöhelyi, A., Kocsis, M., 1980. Surface interaction between H_2 and CO_2 on Rh/Al_2O_3, studied by adsorption and infrared spectroscopic measurements. J. Catal. 65, 428–436.
Spivey, J.J., Egbebi, A., 2007. Heterogeneous catalytic synthesis of ethanol from biomass-derived syngas. Chem. Soc. Rev. 36, 1514.
Storsæter, S., Chen, D., Holmen, A., 2006. Microkinetic modelling of the formation of C_1 and C_2 products in the Fischer–Tropsch synthesis over cobalt catalysts. Surf. Sci. 600, 2051–2063.
Su, J., Mao, W., Xu, X.C., Yang, Z., Li, H., Xu, J., Han, Y.F., 2014. Kinetic study of higher alcohol synthesis directly from syngas over CoCu/SiO_2 catalysts. AIChE J. 60, 1797–1809.
Subramani, V., Gangwal, S.K., 2008. A review of recent literature to search for an efficient catalytic process for the conversion of syngas to ethanol. Energy Fuels 22, 814–839.
Subramanian, N.D., Gao, J., Mo, X., Goodwin Jr, J.G., Torres, W., Spivey, J.J., 2010. La and/or V oxide promoted Rh/SiO_2 catalysts: effect of temperature, H_2/CO ratio, space velocity, and pressure on ethanol selectivity from syngas. J. Catal. 272, 204–209.
van den Berg, F.G.A., Glezer, J.H.E., Sachtler, W.M.H., 1985. The role of promoters in CO/H_2 reactions: effects of MnO and MoO_2 in silica-supported rhodium catalysts. J. Catal. 93, 340–352.
Wang, Y., Luo, H., Liang, D., Bao, X., 2000. Different mechanisms for the formation of acetaldehyde and ethanol on the Rh-based catalysts. J. Catal. 196, 46–55.
Watson, P.R., Somorjai, G.A., 1981. The hydrogenation of carbon monoxide over rhodium oxide surfaces. J. Catal. 72, 347–363.
Yin, H., Ding, Y., Luo, H., Yan, L., Wang, T., Lin, L., 2003. The performance of C_2 oxygenates synthesis from syngas over Rh–Mn–Li–Fe/SiO_2 catalysts with various Rh loadings. Energy Fuels 17, 1401–1406.
Yu, J., Mao, D., Han, L., Guo, Q., Lu, G., 2012. The effect of Fe on the catalytic performance of Rh–Mn–Li/SiO_2 catalyst: a DRIFTS study. Catal. Commun. 27, 1–4.
Yu, J., Mao, D., Han, L., Guo, Q., Lu, G., 2013. Catalytic conversion of syngas into C_{2+} oxygenates over Rh/SiO_2-based catalysts: the remarkable effect of hydroxyls on the SiO_2. J. Mol. Catal. A: Chem. 367, 38–45.
Zaman, S., Smith, K.J., 2012. A review of molybdenum catalysts for synthesis gas conversion to alcohols: catalysts, mechanisms and kinetics. Catal. Rev.: Sci. Eng. 54, 41–132.